LEGIBILITY NOTICE

A major purpose of the Technical Information Center is to provide the broadest dissemination possible of information contained in DOE's Research and Development Reports to business, industry, the academic community, and federal, state and local governments.

Although a small portion of this report is not reproducible, it is being made available to expedite the availability of information on the research discussed herein.

LA-UR -90-564

Los Alamos National Laboratory is operated by the University of California for the United States Department of Energy under contract W-7405-ENG-36

LA-UR--90-564

DE90 007543

TITLE MICROSEISMIC MONITORING OF THE CHAVEROO OIL FIELD, NEW MEXICO

AUTHOR(S) James T. Rutledge
James N. Albright

SUBMITTED TO SPE/DOE Seventh Symposium on Enhanced Oil Recovery

DISCLAIMER

Los Alamos Los Alamos National Laboratory
Los Alamos, New Mexico 87545

Microseismic Monitoring of the Chaveroo Oil Field, New Mexico

by

James T. Rutledge
Consultant

and

James N. Albright
Los Alamos National Laboratory

Submitted February 6, 1990
for presentation at the
SPE/DOE Seventh Symposium on Enhanced Oil Recovery
April 22-25, 1990 Tulsa Oklahoma

ABSTRACT

Microseismicity was monitored in the Chaveroo oil field in southeastern New Mexico during, and for 5 weeks following, a pressurized stimulation of a well being prepared as an injector for a water flood operation. Three-thousand barrels of water were injected into the reservoir over a 5.5-hour period. Little seismicity was detected during the stimulation. Intermittent monitoring over a 5-week period following the injection indicated detectable seismicity occurring with activity levels varying in time. The most active period recorded occurred just after production resumed in the immediate area of the monitor well. Mapping the microearthquakes using the hodogram technique indicates the events occur along linear trends which corroborate known structural trends of the field. Seismicity trends were defined both parallel and perpendicular to the regionally defined maximum horizontal stress direction. Seventy-three good quality events were recorded, in a cumulative 24 hour period, from which structures were mapped up to 3000 ft from the monitor well.

The lack of seismicity during the pressurized injection and the correlation of increased seismicity levels occurring away from an injection well as normal flood production resumed, suggest seismicity is not induced by Mohr-Coulomb failure. We suspect, as has been suggested by previous investigators, that seismicity could be controlled by pressure variations in the reservoir created by the injection and withdrawal of reservoir fluids and local changes in these fluid pressures along preferred flow paths.

INTRODUCTION

The microseismicity of the San Andres Formation in the Chaveroo oil field in southeastern New Mexico was monitored during, and for 5 weeks following, a pressurized stimulation of a well being prepared as an injector for a water flood operation. In addition, the production of tracers injected into the reservoir during the stimulation was measured from nearby wells. The objective of the study was to determine if seismicity was detectable in the San Andres Formation during well stimulation and during normal water flood-production activity at rates practical for mapping the fractures along which microearthquakes occur. Tracers were used to correlate flow paths with trends of seismicity.

Oil is produced from the San Andres Formation in several individual fields that extend over an area of more than 100 miles across the Permian basin of west Texas and eastern New Mexico. The Chaveroo field alone has produced 20.7 million barrels of oil. Generally, oil reservoirs of the San Andres occur locally as 2 to 3 separate zones of porous dolomite. Hydrocarbons are stratigraphically trapped in the formation by porosity pinchouts controlled by dolomitization and anhydrite plugging.[1]

Since 1965, the Chaveroo field has been under primary production and is just beginning to undergo enhanced recovery by water flooding. A common problem of water flooding in the Chaveroo field, as well as other fields producing from the San Andres Formation, is flow anisotropy in the reservoir due to preferred flow along fractures. Premature breakthroughs between injection and producing wells are frequent and reduce oil recovery. If the locations of major fractures in the reservoir were known, then water floods could be designed with well configurations which would delay breakthroughs and improve recovery. The Chaveroo field has wells spaced uniformly at 1320 ft (400 m) in a grid pattern parallel with section boundaries. Pressure interference testing at this well separation has not been successful and the density of wells is insufficient to accurately infer flow direction from breakthrough patterns alone. Microseismic monitoring is an alternative method for determining the location and prevalent orientation of fractures. The method has been successfully used in crystalline rock for mapping

hydraulic fractures.[2,3,4] If the method can be applied in this environment, it could be a useful tool for optimizing water floods in the Chaveroo field and other fields producing from the San Andres Formation.

EXPERIMENTAL SET-UP

The experiment was conducted in Section 34 of the Murphy Operating Corporation's (MOC) Haley Unit of the Chaveroo field (Figure 1). Oil is produced from 3 porosity zones of the Chaveroo field, and in this section they occur over the depth interval 4150-4370 ft (1265-1330 m). Three-thousand barrels of water were pumped into well 34-10 (Figure 1) in the second porosity zone of the Chaveroo field at approximately 4275 ft (1300 m) depth. During the pressurized injection, two 3-component, borehole geophone packages were used for microearthquake detection. Based on regional stress data and a previous tracer experiment conducted by MOC, microseismicity was expected to occur along a NW-SE trend of natural fractures. Expecting this trend, the geophones were placed in wells 34-7 and 34-11 located about 1320 ft (400 m) directly north and west, respectively, from the injection well. Microearthquakes were anticipated to occur in the depth interval of the porosity zones associated with fluid movement in the reservoir. Both geophone packages were stationed at 4200 ft (1280 m) depth. At this depth, the tools were located just above the perforated casing of the first porosity zone putting them close to the expected depth of microseismic activity. Three explosives charges were detonated in shallow holes for orienting the horizontal components of the downhole geophone tools. The first two shots were 4 lbs (1.8 kg) charges detonated near well 34-16, but failed to generate detectable signals. A third, larger charge (20 lbs [9.1 kg]), detonated near well 34-15 was observed on both downhole stations.

Injection took place on June 7, 1989 and lasted 5.5 hours. The pump rate was initially 8.0 barrels per minute and was increased in steps up to a maximum of 10.5 barrels per minute by the end of pumping. These rates corresponded to pressures ranging from 9.6 to 25.7 MPa in excess of hydrostatic pressure over the pumping period. The two tracers were injected with the 3000 barrels of water. Nine-hundred lbs (408 kg) of fluorescein dye were equally distributed in the injection water tanks (3000 barrels total volume) before pumping. Two-hundred lbs (91 kg) of ammonium thiocyanate were injected as a short slug at the start of pumping.

After pumping, the geophone package in well 34-11 was removed. The geophone tool in well 34-7 was left in place to continue monitoring the field for a 5-week period ending on July 13. Immediately following the pressurized injection, Section 34 of the field was shut down for 12 days. On June 19, Section 34 was put back on normal production with the injection well 34-10 taking 250 barrels per day under hydrostatic pressure. Pressures at the depth of the injection (approximately 4300 ft [1310 m]) was about 12.8 MPa when the tubing column was full to the surface. On July 5, wells 34-2, 34-4, and 34-12 were also put on line as water injectors, each taking about 200 barrels per day under hydrostatic pressure.

Data were recorded on analog tape throughout the pressurized injection of June 7 and for several hours thereafter. Monitoring during the 5 following weeks was not continuous. Post-injection data were recorded using both analog tape and a digital event recorder. The digital recorder stored signals captured by an algorithm which triggered on signal levels of a specified amount over a continuously-measured, background level. On the average, the memory capacity of the digital recorder filled in about 40 hours. The total time covered by the digital recorder was 315 hours over the 5 weeks following injection. An additional 76 hours of coverage was recorded on analog tape on 7 different nights. Night recordings had substantially less noise than daytime recordings. Unlike the digital data, the analog tapes give a continuous record of the geophone output. Subsequent digitization of the analog records using more sensitive triggering algorithms

and higher sampling rates, provided the increased signal bandwidth required for analysis and allowed detection of microearthquakes too small to trigger the digital recorder that was used in the field.

TRACER DATA

Ten wells of Section 34 were sampled daily for tracer content after production resumed on June 19. From June 19 to late-July, the fluorescein dye was detected in small quantities (a maximum of 5 ppm) which were near the limit of its detectability in the reservoir water . The ammonium thiocyanate was not detected at all. Sampling was reduced in late August to once a week. In the 7 months since injection, the dye has not been detected again. If the measured fluorescein levels are accurate, then the negative results for thiocyanate would be expected since less was injected and the analytical sensitivity is less than that of the dye. But, since the fluorescein measurements are equivocal, it is possible that neither tracer was, or will be, detected. Possible explanations for no detection are: 1) the tracers were adsorbed on the rock surfaces, 2) the transit times between wells are very long for the injection and production rates used in the section, 3) transit times are fast enough for the tracers to have been missed, or 4) the concentrations of the tracers were diluted below detection limits. Adsorption is possible, but not likely considering that these two tracers are commonly used in oil reservoirs, and are known not to exhibit significant adsorption. Tracer dilution does not seem to be very likely either, considering the large quantities of tracer injected. The two most plausible explanations are opposites. Fluid transit times could have been fast enough that the tracers were produced in adjacent areas of the field which were producing during the 12 days Section 34 was shut down. This would imply that flow in the reservoir is highly anisotropic and occurs predominantly along a few highly conductive fractures. The opposite explanation, that fluid transit times are long enough in the reservoir to have produced no tracer, suggest that there are no direct flow paths connecting the injector with any of the producing wells that were sampled.

SEISMIC DATA

The an g field tapes were played back through a computer based, data-acquisition system. Micro hquake signals triggering the system were digitized at a sample interval of 0.2 ms. The data recorded digitally in the field were limited to a minimum sample interval of 2.0 ms. The digital field recorder had built in anti-alias filters low passing below 250 Hz. Input to the digital recorder was high-pass filtered at 50 Hz to remove low-frequency noise observed in the field. Geophone output was recorded on analog tape without filtering. An anti-alias filter was applied during subsequent digitizing. A noise source in the field persisted throughout the whole experiment. The noise had a cycle of approximately 20 minutes on - 20 minutes off and a frequency bandwidth comparable to that of the seismic signals. Useful data acquisition time in the field was therefore effectively cut in half. The noise source may have been a gas compressor facility located one mile east of monitor well 34-7 where gas is gathered and compressed to line pressure for distribution. The trigger sensitivity of the field recorder was lowered to avoid filling the memory with noise events.

Signals resulting from microseismic events were selected by visually inspecting plots of all discrete signals that were recorded. Microearthquakes were identified as signals with clearly defined compressional (P) wave and shear (S) wave arrivals. One-hundred-fifty-four events were selected from the analog data and 115 events from the field digital data. The time distribution of the event occurrences for the two data sets are shown in Figures 2 and 3. Monitoring was not continuous over the 5 weeks following injection resulting in large gaps when data was not gathered. Only 4 events were detected during the 5.5-hour, pressurized injection and these events were only detected in well 34-7. The sensitivity of the second geophone

package was less, and apparently too small, to detect the few events recorded in well 34-7. The digital event recorder operated for the two days immediately following the injection, but triggered during the noise periods so frequently that only 4 microearthquake events were detected. Trigger sensitivity was then lowered to prevent the complete filling of memory during the noise periods. Because the recorder sensitivity level was different for these two days, these four events are not included in Figure 3. The computer algorithm used in digitizing the analog data enabled the detection of more microearthquakes over shorter intervals of time than was possible from the field digital-recorder.

Most of the microearthquakes that were observed occurred during the period June 19-23. Since there are gaps in the data acquisition, it is not known when the microearthquake activity in the section actually peaked or how it fluctuated throughout the 5 weeks. It is interesting to note, however, that the maximum seismic activity which was measured occurred immediately after Section 34 of the field was put back on production. Both data sets show decreasing seismic activity from the high of June 19 until July 1 when the field digital recorder showed an increase in activity. The analog data recorded after June 23 is contaminated by high frequency noise of unknown origin, which, because the signal-to-noise ratio of events is lowered, makes triggering the data acquisition system more difficult. The field digital data was not affected by the higher frequency noise because of the anti-alias filters.

The three components of particle velocity and a displacement amplitude spectrum of a representative event are shown in Figure 4. The vertical component recorded higher frequencies than the two horizontal components. Typically, the horizontal components of 3-component, borehole, geophone tools resonate differently than the vertical component. The resonance of the vertical component is effected by rigid body motion that depends predominantly on tool length, while the resonances of the horizontal components are sensitive to the coupling of the geophone package to the wellbore.[5]

Like the sample spectrum shown in Figure 4, the displacement amplitude spectra in general have a typical shape of a shear-slip seismic event. The corner frequencies range between about 50 and 90 Hz, which are an order of magnitude lower than corner frequencies of microseismic events measured in crystalline rock.[6] The lower corner frequencies observed in this environment may be due to larger source areas and/or lower seismic Q of the rocks. The spectra's frequency roll off above the corner ranges between ω^{-2} and ω^{-3},where ω is angular frequency. This value range is also typical of shear-slip seismic events.

DATA ANALYSIS AND RESULTS

Microearthquake Locations

Mapping microearthquakes recorded at two or more locations can be accomplished by using P- and S-wave arrival times alone. If the velocity structure is known accurately, microearthquake locations can be determined uniquely from P- and S-wave arrival times with detection at at least 3 stations. Having only recorded events at one 3-component station, we are limited to mapping using the hodogram technique in which distance is determined from the S-P arrival time difference, and direction to the event is determined from the P-wave particle motion of the first arrival. Direction to the event is parallel to the major axis of an ellipsoid fitted to the 3-dimensional seismic particle motion.[7] We have applied the method in 2-dimensions by fitting an ellipse to the horizontal components of particle motion. A sample hodogram of the P-wave arrival from an event is shown in Figure 5. Major and minor axes are shown in Figure 5 for the best fitting ellipse to the horizontal particle motion. The vertical component was not used because it contains strong resonance at higher frequencies than the horizontal components, and

its first arrivals have a relatively poor signal-to-noise ratio. The degraded signal-to-noise ratio results from consistently smaller P-wave arrivals on the vertical axis, as seen in Figure 4. First arrivals from the orientation shot at the surface have a much stonger P-wave arrival on the vertical component than on the horizontals as would be expected with its steep incidence. The smaller vertical-component, P-wave arrivals for the microearthquakes, implies that seismicity is restricted to depths close to the geophone depth. This seems reasonable if seismicity is occurring due to strain release resulting from fluid movement in the porosity zones of the reservoir.

For computing distance, a P-wave velocity of 19,800 ft/s (6040 m/s) was used. This value was determined from sonic logs of wells 34-7 and 34-10 by averaging over the 3 porosity zones of the field. A value of 1.75 was used for the ratio of P-wave velocity to S-wave velocity. This is a reasonable number for brine-saturated dolomites and anhydrites with this high a velocity.[8]

The data that were digitally acquired in the field were too under-sampled for applying the hodogram technique. Only the digitized analog data were used. These data were edited based on the ellipticity of the hodograms. Events with an ellipse-trajectory aspect ratio less than 4.0 were eliminated for mapping purposes. The high frequency noise contaminating the data late in the experiment, mentioned above, resulted in no mappable events after June 27. Seventy-three events were selected, all of which occurred on the nights of June 19 and 23 (Figure 2). None of the 4 events occurring during the pressurized injection of June 7 had a sufficiently reliable hodogram trajectory for mapping. The first 2 ms of P-wave particle motion, about one-half of a cycle, were used in hodogram trajectory measurements. Lengthening the first arrival data used increasingly aligns event trajectories 45° to the horizontal components. We suspect that a strong geophone-site response causes the event trajectories to align at 45° from the two axes. The effect is minimized by using only the first half cycle of particle motion.

Figure 6 shows the locations of events that occurred on the nights of June 19 and 23. The map indicates microearthquakes occurred along two orthogonal trends running NW-SE and NE-SW. Events were detected up to 5600 ft from monitor well 34-7 but most occurred within 3000 ft. There is a 180° ambiguity in locating events from one downhole, receiving station since its position relative to shear motion at the microearthquake source is unknown. An observed first motion may be a compression first arrival from the indicated direction or a rarefaction first arrival from the opposite direction. We have plotted all events to the SW of monitor well 34-7 so that they are located closest to injection well 34-10. Some or all of the microearthquakes could just as well be occurring to the NE of the monitor well. If the events were plotted on either side, the azimuthal trends of seismicity would not change. In a test, we assumed that all first motions were compressive, so that events plotted on each side of the monitor well. Both trends indicated in Figure 6 could be identified symmetrically about the monitor well. The unlikely possibility of a seismicity gap between the monitor well and NW-SE trends spaced equally on each side of the well suggest that most events are occurring to one side or the other of the geophone station and, if so, that the displacement direction along fractures is not always in the direction.

l events were rotated to geographic coordinates by determining the location of the orientation ot via the hodogram technique. As with the event trajectories, a half cycle (14 ms) of the shot t arrival was used. The trajectory ellipse passed our criteria of requiring an aspect ratio ater than 4, but the signal-to-noise ratio of the horizontal components was poor because shot rgy, coming from the surface, had a steep vertical incidence. Therefore, the absolute ntation of seismicity is not known with good accuracy, and added to the 180° location iguity discussed above, makes the interpretation of seismic event locations necessarily ted. Nonetheless, trends can be identified, and these trends, as best as can be mapped, do borate prior knowledge of the field. Regional stress data from this area indicates a

maximum horizontal stress oriented NW-SE so that microseismicity induced by fluid flow would be expected to occur along a NW-SE trend.[9] A previous tracer test conducted by MOC in the section immediately west of the experiment site indicated a flow preference along natural fractures oriented NW-SE. Premature breakthrough observations during flooding operations have also indicated fractures oriented in the opposite direction, NE-SW, in nearby parts of the San Andres Formation.[10] The NE-SW trend of seismicity is especially well defined by mapping only the events occurring the night of June 19. During an observation period of 13 hours, two distinct, parallel trends striking NE-SW along with the conjugate NW-SE trend are imaged (Figure 7).

Seismic Recurrence Rate

From an engineering viewpoint, quantifying the recurrence rate of seismicity in an oil field is of use in predicting the time necessary to record a given number of mappable microearthquakes in a desired area of the field. Graphically, the recurrence can be represented as a b-value plot which measures the number of small events occurring relative to the number of large events occurring. The b-value is the slope of the regression line for the data fitted to equation

$$\log N = a - bm \qquad (1)$$

where N is the cumulative number of events of magnitude m or larger. We computed a b-value of 0.63 over a relative scale of 2 orders of magnitude (Figure 8). Our relative magnitude scale is a pseudo-magnitude scale computed similar to Aki.[11] Magnitude is taken as the log of amplitude measured at a fixed lapse time from the coda decay curve of each event. Figure 8 represents the recurrence of those events occurring over a cumulative 24-hour monitoring time on the nights of June 19 and 23 (13 and 11 hours, respectively). The b-value computed is probably effected by the geophone location. Little seismicity is occurring within 1500 ft of the monitor well. Had the geophone been placed closer to the region of seismicity, more smaller magnitude events would have been detectable, thereby increasing the b-value. The threshold of detection, represented where the curve flattens at smaller magnitudes, might also be lowered with a closer geophone position if such events are occurring.

Figure 9 shows the magnitude limit of detection as a function of distance. At 3000 ft, for instance, events with relative magnitudes less than -0.7 are not likely to be detected. Relating this limit to Figure 8, one could, in concept, predict the cumulative number of events detectable within 3000 ft of a geophone station over some time interval. The seismicity has not been characterized accurately enough in this field area to make such a prediction. We can conclude, however, that detectable seismicity did occur in the Chaveroo field during normal production and can be shown to occur along linear trends. Also, enough events were obtained within a cumulative 24-hour period for mapping structures up to 3000 ft from the monitor well. Considering that one half the monitoring time was contaminated by periodic noise, the effective recording time of the 73 mappable events detected is 12 hours. This is generally true because the rate of seismicity was evenly distributed over the two respective monitoring periods.

The temporal variation of seismicity that was observed (Figures 2 and 3) should be understood before any predictions of when microearthquakes will occur in the Chaveroo field can be made. Of particular interest is why little seismicity was detected during pressurized injection and most occurred soon after production in the field resumed. The model usually used to explain induced seismicity is Mohrs-Coulomb failure in which shear failure occurs when fluid pressure exceeds some critical level. With this model, seismicity would be expected to occur in high pressure areas close to the injection well as soon as pressure had built up over sufficient areas. On larger time and spatial scales, Pennington et al.[12] and Davis and Pennington[13] apply the barrier-asperity

model to explain earthquake occurrence in water flooded oil fields of Texas. In this model, strength varies over areas of a fault. High strength areas (barriers) of the fault can be stress loaded by seismic or aseismic slip along weaker sections of the fault causing the high strength areas to become high stress areas (asperities). Earthquakes occur when asperity strengths are exceeded. Applying this model to a water-flooded oil field, Davis and Pennington[13] show that the variations of effective rock strength over the field area induced by the injection and withdrawal of reservoir fluids are significant enough for earthquakes to occur by this mechanism. In contrast to the Mohr-Coulomb model, seismicity occurs in low fluid pressure areas of fluid withdrawal where the effective strength of the rock is increased, and stress loading occurs by the coupling of stress released aseismically in high pressure areas of the field where fluid is injected. We speculate that, on a smaller scale, pressure variations between injector and producing wells are controlling the microseismicity that is observed. Seismicity in this case can be delayed from the time of injection until either stress loading exceeds asperity strength or locally increased pressure lowers the effective strength of asperities. During flooding, local pressure increases should occur along preferred flow paths.

All producing wells of Section 34 were shut down during the pressurized injection. Nearly all of the microseismicity detected in the field occurred just after production resumed on June 19, with the injection well 34-10 taking water under hydrostatic pressure. The paucity of microearthquakes during the pressurized injection and then the relative abundance of microeathquakes occurring where pressures would be expected to be relatively low in the reservoir (Figure 6), suggest a pressure-controlled, barrier-asperity model of induced seismicity. If so, microearthquakes have probably been induced during flooding by local pressure increases along preferred flow paths, lowering the effective strength of the rock where stresses have accumulated. It is not known if stresses released during the pressurized injection aseismically, or at least below the detection threshold, are coupled to later stress release manifested as microearthquakes. The stress release resulting in microearthquakes could just as well have accumulated from strength variations along fractures induced by normal production in the field. A more robust experiment is needed to verify if indeed microearthquakes are occurring in low pressure areas of the reservoir and to more accurately monitor how microseismicity varies with production activity. Specifically, constant monitoring time capability at several downhole geophone stations (at least 3) is needed to produce an accurate microearthquake location map and reliably characterize seismic recurrence in the field. In addition, a successful tracer experiment should be conducted in conjunction with seismic monitoring to correlate flow paths with the seismic stress release along fractures. Finally, we believe that modeling pressure variations in the field, using tracer data and individual well production-injection volumes, may explain the mechanism causing microearthquakes and thereby provide an understanding of the temporal variation of microseismicity in the field.

CONCLUSIONS

Microseismic monitoring of the Chaveroo oil field during a 3000-barrel pressurized injection of water over a 5.5-hour period resulted in little detectable seismicity.

Intermittent monitoring over a 5-week period following the injection indicated detectable seismicity occurring with activity levels varying in time. The most active period recorded occurred just after production resumed in the section. Monitoring during the 5 weeks was not complete enough to draw general conclusions on temporal variations of seismicity.

Mapping the microearthquakes using the hodogram technique indicates the events occurring along linear trends which corroborate known structural trends of the field. Seismicity trends were defined both parallel and perpendicular to the regionally-defined maximum, horizontal

stress direction. Seventy-three good quality events were recorded in a cumulative 24-hour period from which structures were mapped up to 3000 ft from the monitor well.

Two chemical tracers were pumped into the reservoir during the pressurized injection. After 7 months, the fluorescein dye has not yet been detected at levels considered above noise of the analytical measuring technique. The ammonium thiocyanate has not been detected at all. The reason for the failure to recover tracer is not known.

The lack of seismicity during the pressurized injection and the correlation of increased seismicity levels occurring away from an injection well as normal flood production resumed, suggest seismicity is not induced by Mohr-Coulomb failure. We suspect, as have previous investigators, that seismicity could result from pressure variations in the reservoir created by the injection and withdrawal of reservoir fluids and the local changes in these fluid pressures along preferred flow paths.

ACKNOWLEDGMENT

The field experiment was a collaborative effort between Los Alamos National Laboratory and the Murphy Operating Corporation (MOC) working under the auspices of the DOE's Oil Recovery Technology Partnership. We are grateful for MOC's invitation to carry out this work and their support in the field. Special thanks goes to Mark B. Murphy of MOC for his cooporation and contributions throughout this project. We also gratefully acknowledge Robert J. Hanold, co-Chairman of the Partnership, who encouraged us to undertake the project and contributed to its planning and execution.

REFERENCES

1. Cowan, P.E. and Harris, P.M.: "Porosity Distribution in San Andres Formation (Permian), Cochran and Hockley Counties, Texas," Ameican Association of Petroleum Geologist Bulletin (July 1986) v. 70, p. 888-897.

2. Albright, J.N. and Pearson, C.: "Acoustic Emissions as a Tool for Hydraulic Fracture Location," Society of Petroleum Engineers Journal (1982) p. 523-530.

3. Pine, R.J. and Batchelor, A.S.: "Downward Migration of Shearing in Jointed Rock During Hydraulic Injection," International Journal of Rock Mechanics, Mining Science and Geomechanical Abstracts (1984) v. 21, p. 249-263.

4. Fehler, M., House, L. and Kaieda, H.: "Determining Planes Along Which Earthquakes Occur: Method and Application to Earthquakes Accompanying Hydraulic Fracturing," Journal of Geophysical Research (Aug. 1987) v. 92, p. 9407-9414.

5. R. Baria, Camborne School of Mines, Cornwall, U.K.: personal communication, (Nov. 1989).

6. Fehler, M., House, L. and Kaieda, H.: "Seismic Monitoring of Hydraulic Fracturing: Techniques for Determining Fluid Flow Paths and State of Stress Away from a Wellbore," Proceedings of the 27th U.S. Rock Mechanics Symposium (1986).

7. Matsumura, S.: "Three-Dimensional Expression of Seismic Particle Motions by the Trajectory Ellipsoid and its Application to the Seismic Data Observed in the Kanto District, Japan," Journal of the Physics of the Earth (1981) v. 29, p. 221-239.

8. Rafavich, F., Kendall, C.H. St. C. and Todd, T.P.: "The Relationship Between Acoustic Properties and the Petrographic Character of Carbonate Rocks," Geophysics (1984) v. 49 p. 1622-1636.

9. Aldrich, Jr., M.J. and Laughlin, A.W.: "A Model for the Tectonic Development of the Southeastern Colorado Plateau Boundary," Journal of Geophysical Research (Nov. 1984) v. 89, p. 10207-10218.

10. M. B. Murphy, Murphy Operating Corporation, Roswell, New Mexico: personal communication, (Jan. 1990).

11. Aki, K.: "Physical Basis for the Duration Magnitude and Recommended Practice for Coda Magnitude Determination," Proceedings of the 17th Assembly of the ESC, Budapest, (1980).

12. Pennington, W.D., Davis, S.D., Carlson, S.M., DuPree, J., and Ewing, T.E.: "The Evolution of Seismic Barriers and Asperities Caused by the Depressuring of Fault Planes in Oil and Gas Fields of South Texas," Bulletin of the Seismological Society of America (Aug. 1986) v. 76, p. 939-948.

13. Davis, S.D. and Pennington, W.D.: "Induced Seismic Deformation in the Cogdell Oil Field of West Texas," Bulletin of the Seismological Society of America (Oct. 1989) v. 79, p. 1477-1495.

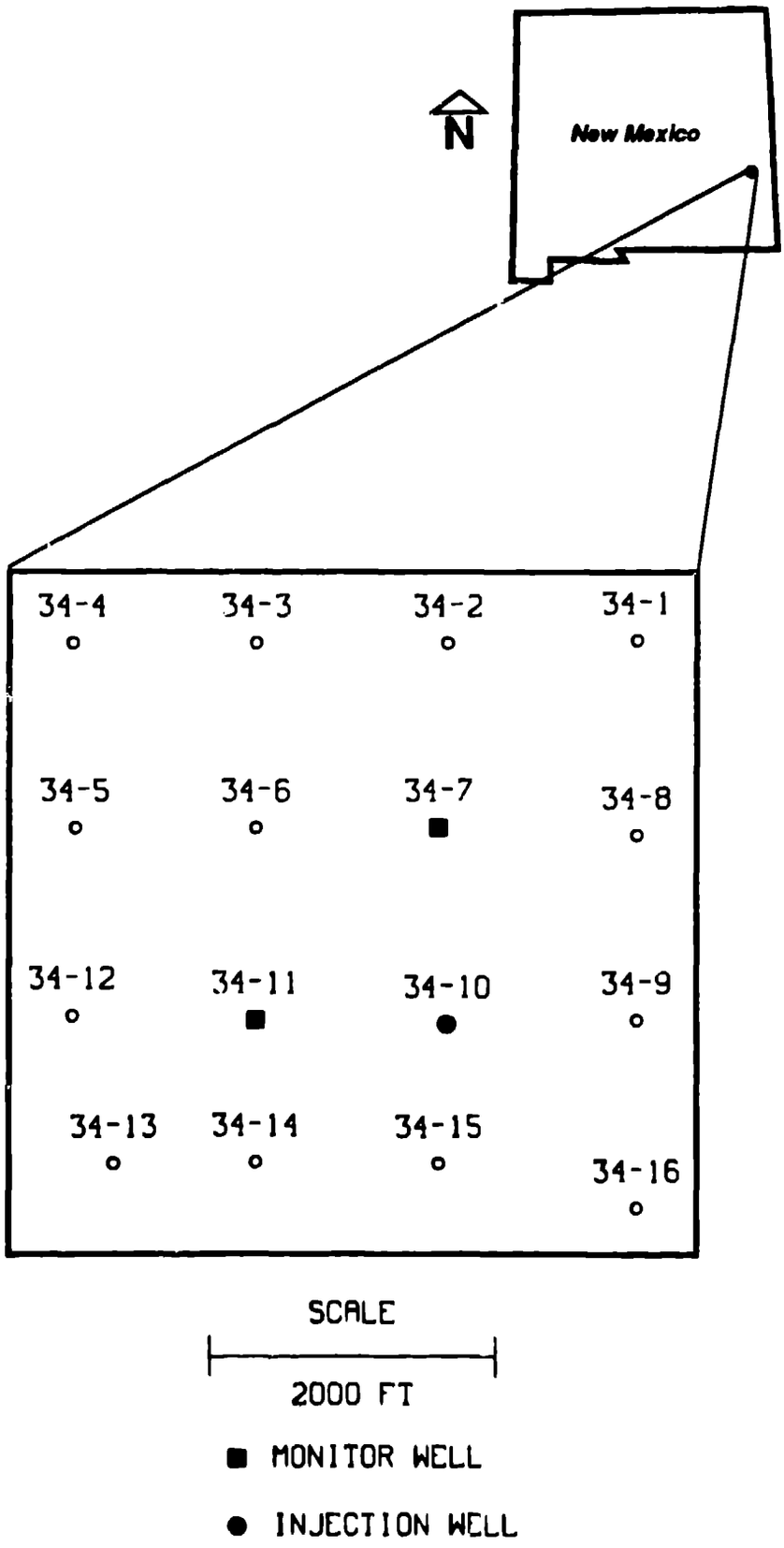

Figure 1. General location map and the well configuration of Section 34 of the Murphy Operating Corporation's Haley Unit of the Chaveroo oil field, New Mexico.

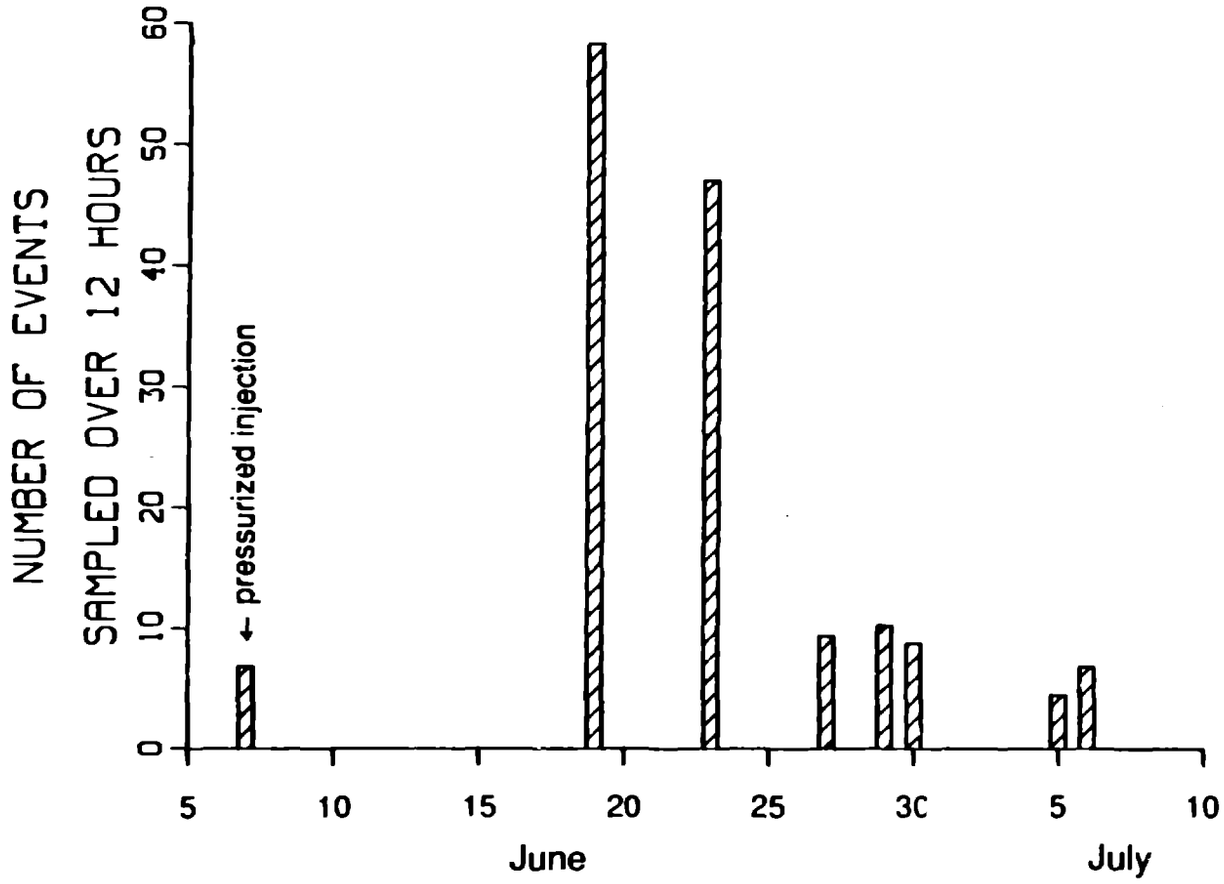

Figure 2. Number of microearthquakes detected from analog tape normalized to the average duration of the recording sessions (12 hours).

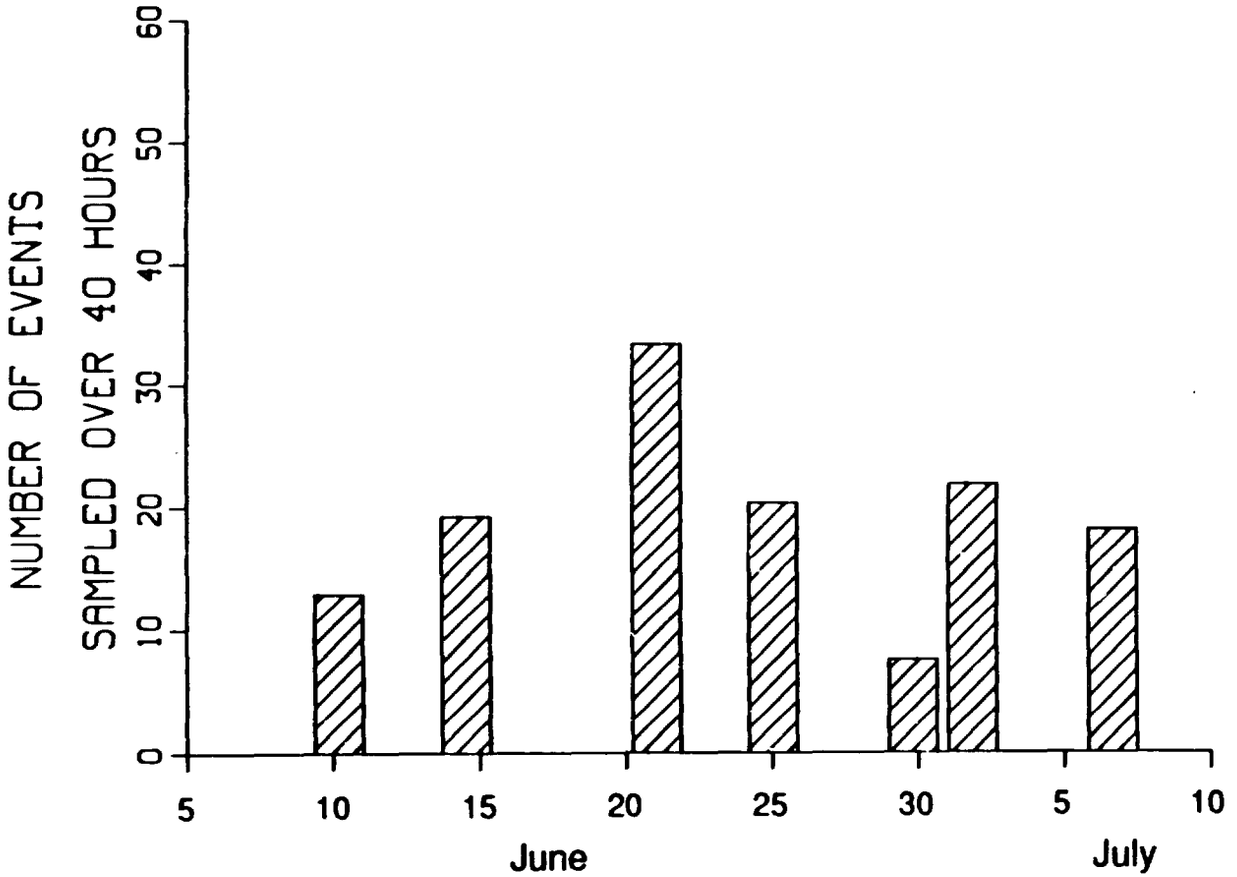

Figure 3. Number of microearthquakes detected by the field digital event recorder normalized to the average duration of the recording sessions (40 hours).

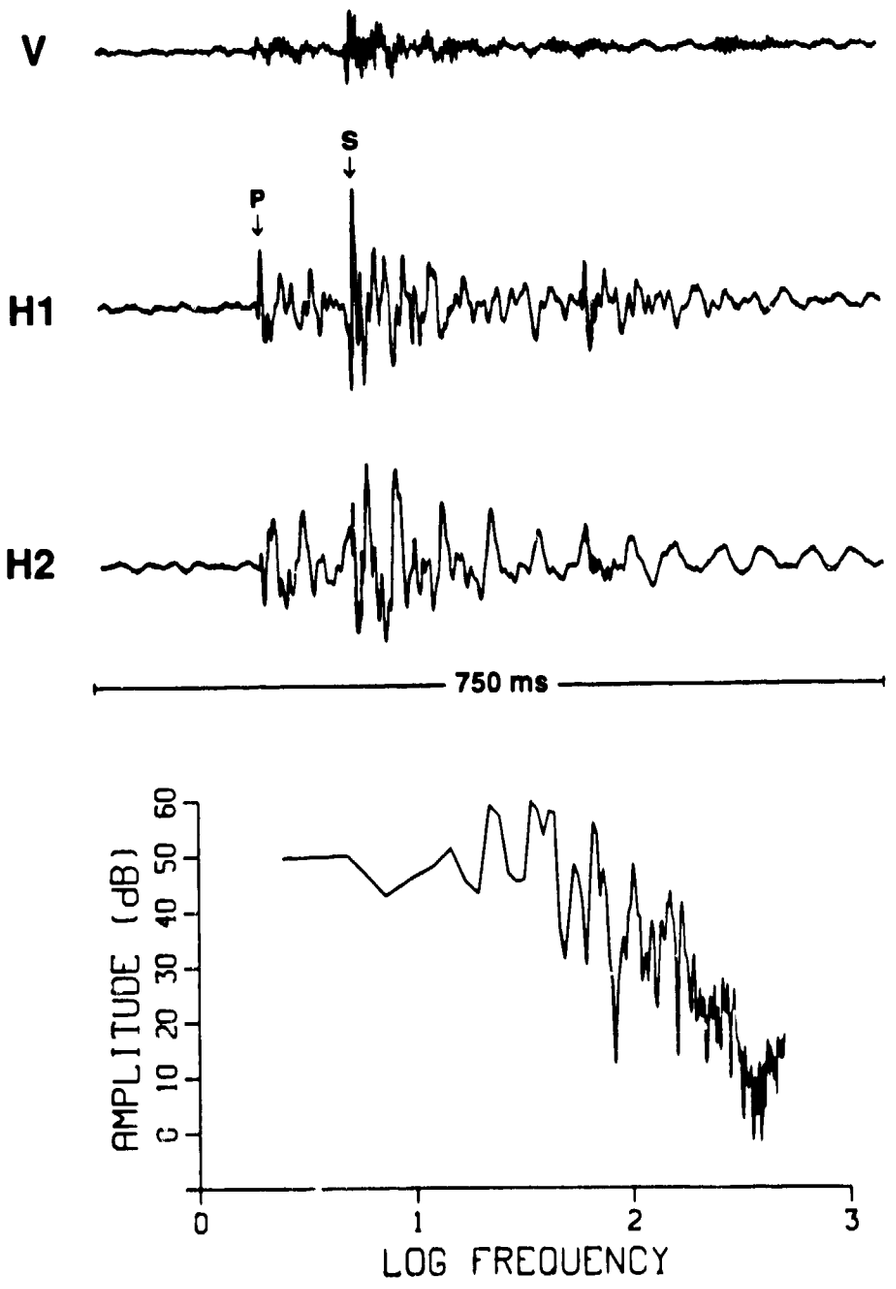

Figure 4. Three components of a typical microseismic event detected (above) and the displacement amplitude spectrum of the P- and S-wave of the horizontal component H1 (below).

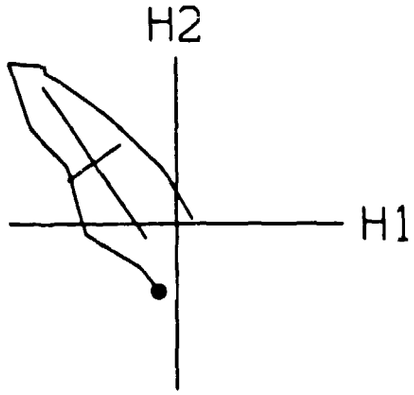

Figure 5. Two milliseconds of the horizontal-component, P-wave particle motions for the event shown in Figure 4. Major and minor axes of the best fitting ellipse to the particle motion are shown.

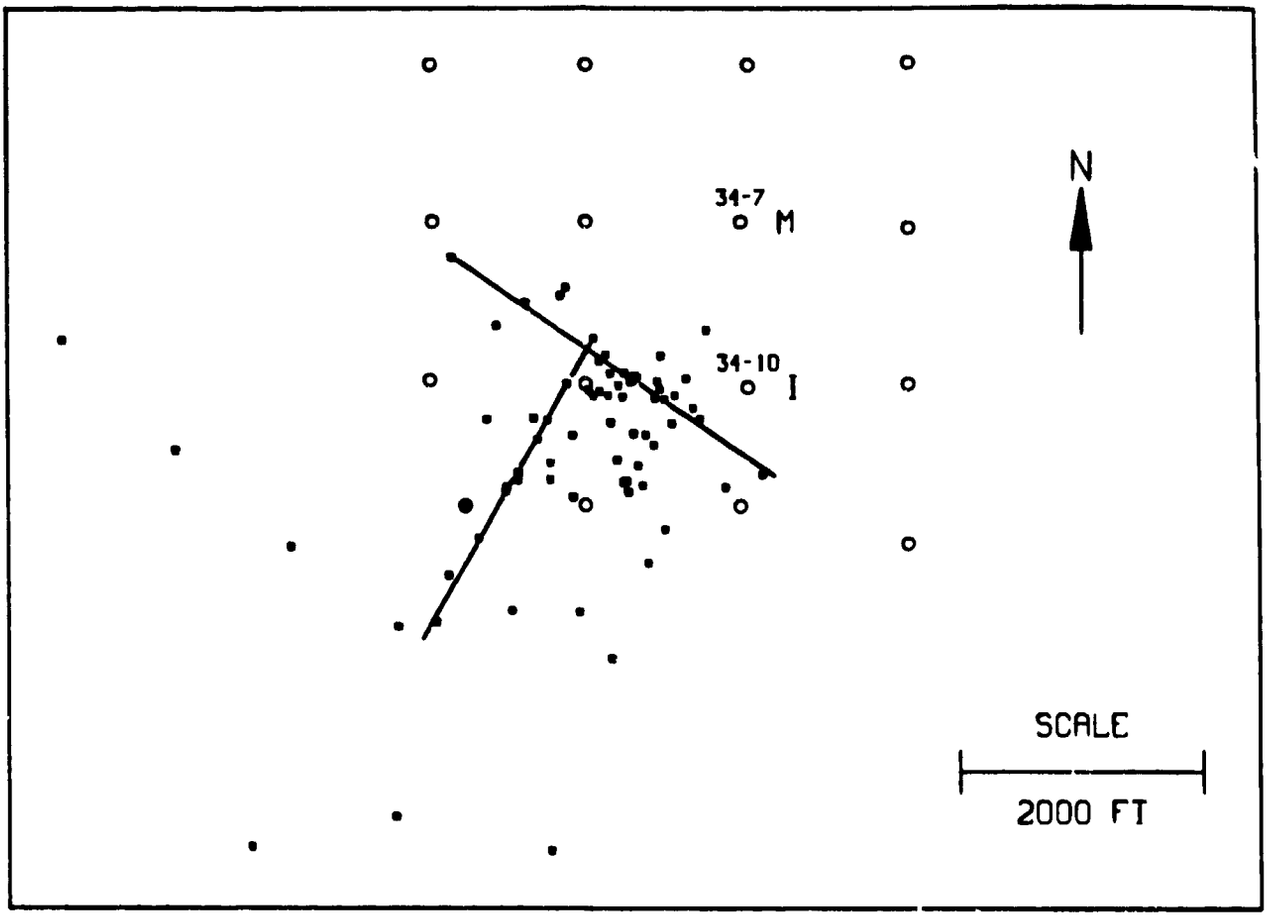

Figure 6. Microearthquake location map for events detected on June 19 and 23 shown with the interpreted trends and the wells of Section 34.

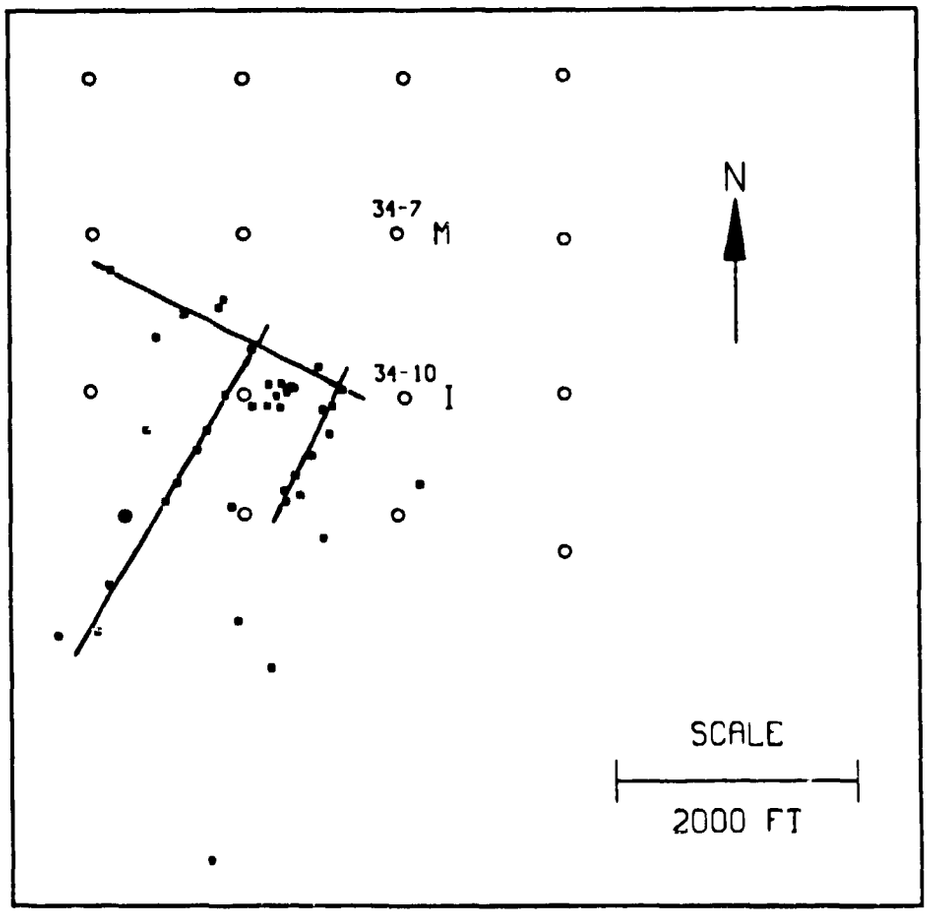

Figure 7. Microearthquake location map for the events detected on June 19.

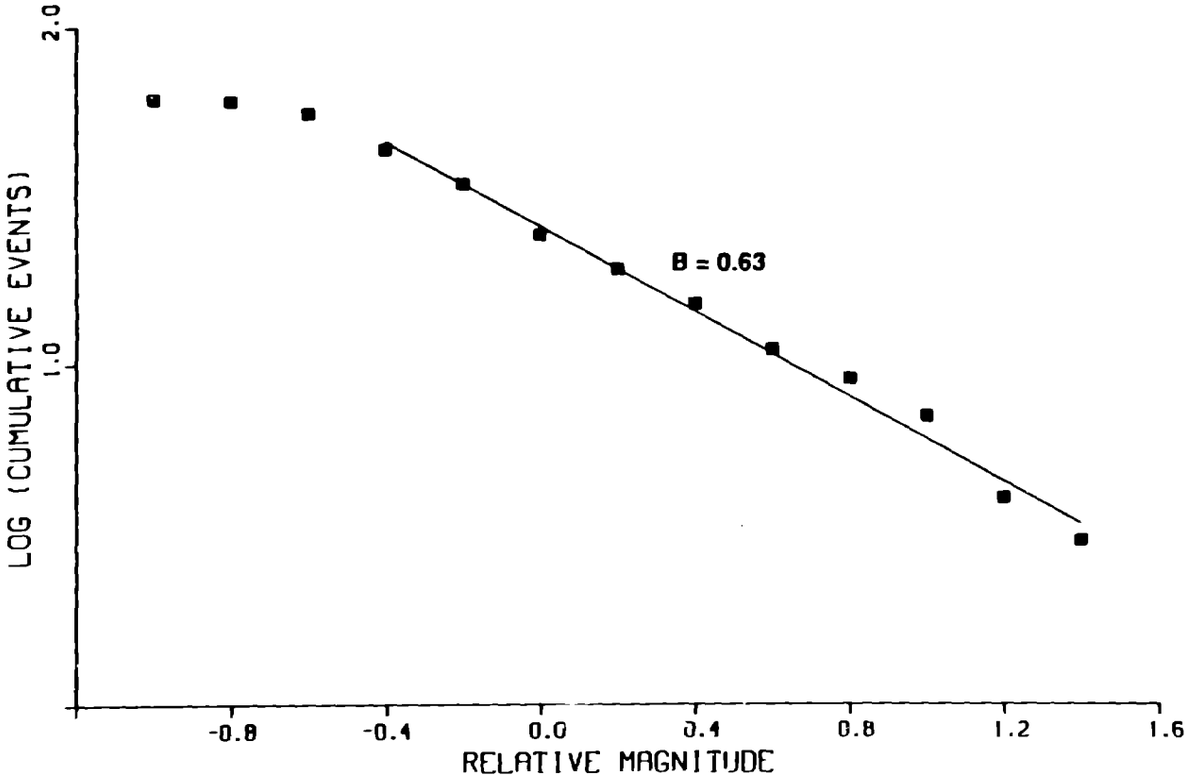

Figure 8. B-value plot for the microearthquakes detected on June 19 and 23.

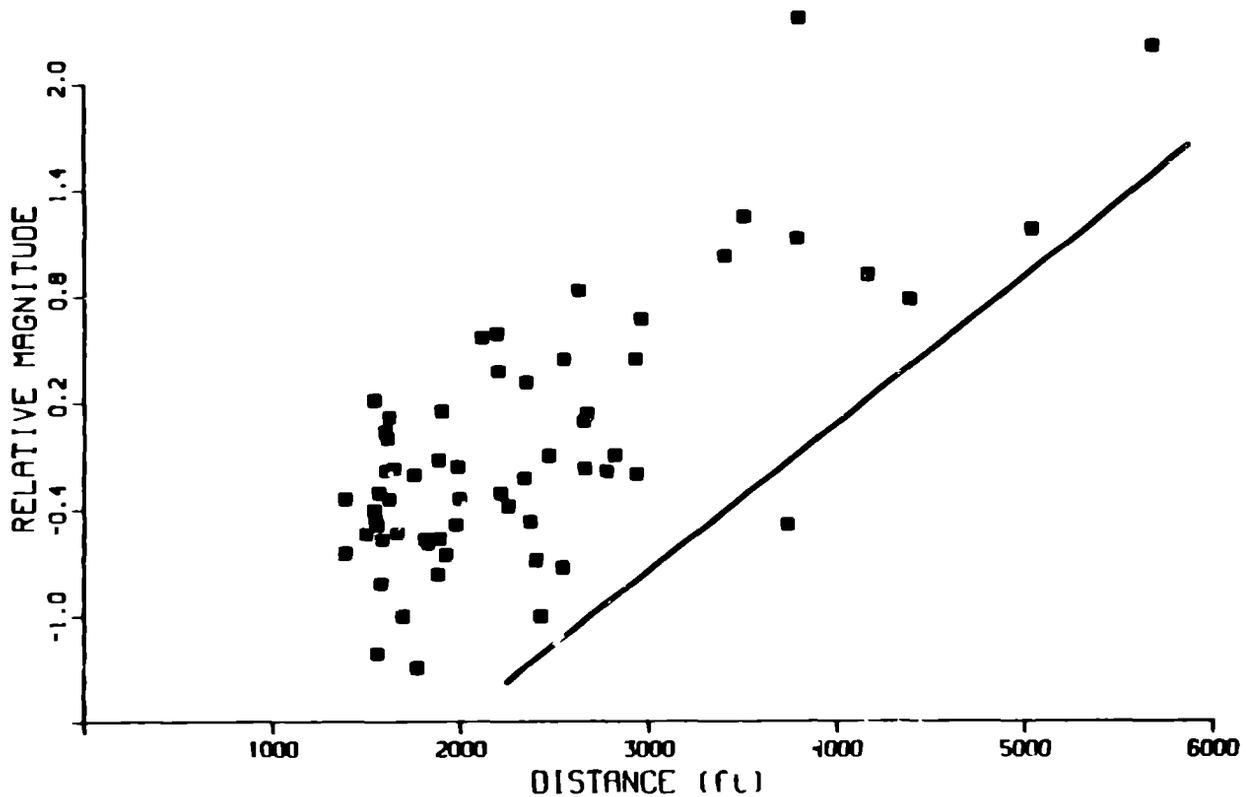

Figure 9. Magnitude versus distance plot for the microearthquakes detected on June 19 and 23. The line shows the relative-magnitude limit of detectability as a function of distance.